Continuous Pathway between the Elasto-Inertial and Elastic Turbulent States in Viscoelastic Channel Flow

Mohammad Khalid,[1] V. Shankar,[1,*] and Ganesh Subramanian[2,†]
[1]Department of Chemical Engineering, Indian Institute of Technology, Kanpur 208016, India
[2]Engineering Mechanics Unit, Jawaharlal Nehru Center for Advanced Scientific Research, Bangalore 560084, India

(Received 22 March 2021; revised 18 June 2021; accepted 27 August 2021; published 22 September 2021)

Viscoelastic plane Poiseuille flow is shown to become linearly unstable in the absence of inertia, in the limit of high elasticities, for ultradilute polymer solutions. While inertialess elastic instabilities have been predicted for curvilinear shear flows, this is the first ever report of a purely elastic linear instability in a rectilinear shear flow. The novel instability continues up to a Reynolds number (Re) of $O(1000)$, corresponding to the recently identified elasto-inertial turbulent state believed to underlie the maximum-drag-reduced regime. Thus, for highly elastic ultradilute polymer solutions, a single linearly unstable modal branch may underlie transition to elastic turbulence at zero Re and to elasto-inertial turbulence at moderate Re, implying the existence of continuous pathways connecting the turbulent states to each other and to the laminar base state.

DOI: 10.1103/PhysRevLett.127.134502

Dilute polymer solutions undergo two different transitions to novel turbulent states, both driven by viscoelasticity, and thence, fundamentally distinct from the now well-understood Newtonian transition [1–3]. Pipe and channel flows of sufficiently elastic polymer solutions transition from the laminar state at Reynolds numbers substantially lower than the typical Newtonian threshold, the ensuing flow state dubbed elasto-inertial turbulence (EIT) to emphasize the importance of both elastic and inertial effects underlying the turbulent dynamics [4–10]. The EIT state is dominated by spanwise oriented 2D structures [8,11] in sharp contrast to the Newtonian scenario [2], and for plane Poiseuille flow, has recently been shown [12,13] to be connected subcritically to a linear center-mode instability [14–16]; recent pipe-flow experiments have, in fact, found remarkable agreement between the observed structures at EIT onset [7] and the center-mode eigenfunction [14,15]. On the other hand, curvilinear shearing flows of dilute polymer solutions transition to elastic turbulence (ET) in the inertialess limit [17–19], the transition being triggered by a hoop-stress-driven linear instability [20–27]; the eventual disorderly ET state that arises has been well characterized experimentally [17,18,27] and, to a limited extent, theoretically as well [28].

Unlike their curvilinear counterparts, inertialess rectilinear shear flows of dilute polymer solutions have hitherto been regarded as linearly stable [29–31]. Transition in these flows has been proposed to occur via a subcritical mechanism, but one that nevertheless involves a hoop stress that now arises at a nonlinear order due to the curvature of the perturbed streamlines [32–36]. There is some experimental evidence of an inertialess finite-amplitude transition [32,37–39] to what might be an ET state similar to that observed for curvilinear flows; the absence of a linear instability has also motivated examination of nonmodal growth mechanisms, both in the absence [40,41] and presence [42] of inertia. The aforementioned EIT and ET states might seem unrelated at first sight, on account of fluid inertia playing a fundamental role in the former, while being irrelevant in the latter. It has nevertheless been speculated [4,7,12,19,39] that the two states may be linked, although there exist no concrete hypotheses or proposals in this regard.

In this Letter, we show that (i) pressure-driven viscoelastic channel flow is linearly unstable even in the absence of inertia, making this the first ever report of a purely elastic linear instability not dependent on base-state streamline curvature; (ii) the instability smoothly continues, with increasing Reynolds number (Re), to the aforementioned elasto-inertial linear instability [14,16]. Since the latter instability has been shown to subcritically continue to nonlinear elasto-inertial coherent structures [12,13], the implication is the existence of a continuous pathway (the underlying unstable modal branch) connecting the EIT and ET states, one that might provide a template for nonlinear coherent structures acting as possible bridges between these states, thereby forming the framework for a dynamical-systems-based interpretation of turbulence outside the Newtonian realm.

We consider pressure-driven flow of an incompressible viscoelastic fluid in a channel of width $2H$. The governing mass and momentum equations [43,44], in dimensionless form, are

$$\boldsymbol{\nabla}\cdot\mathbf{u}=0,\quad \mathrm{Re}\left(\frac{\partial\mathbf{u}}{\partial t}+(\mathbf{u}\cdot\boldsymbol{\nabla})\mathbf{u}\right)=-\boldsymbol{\nabla}p+\beta\nabla^2\mathbf{u}+\boldsymbol{\nabla}\cdot\boldsymbol{\tau}, \qquad (1)$$

where $\mathbf{u}$, p, and $\boldsymbol{\tau}$, are the velocity, pressure, and the polymer stress fields, respectively. Here, lengths are nondimensionalized using the channel half-width H, velocities using the base-flow maximum $U_{\max}$, and $\boldsymbol{\tau}$ is governed by the Oldroyd-B constitutive relation

$$\boldsymbol{\tau} + W\left(\frac{\partial \boldsymbol{\tau}}{\partial t} + (\mathbf{u}\cdot\boldsymbol{\nabla})\boldsymbol{\tau} - (\boldsymbol{\nabla}\mathbf{u})^T\cdot\boldsymbol{\tau} - \boldsymbol{\tau}\cdot(\boldsymbol{\nabla}\mathbf{u})\right) = (1-\beta)(\boldsymbol{\nabla}\mathbf{u} + \boldsymbol{\nabla}\mathbf{u}^T). \quad (2)$$

The relevant dimensionless groups are the Reynolds number $\mathrm{Re} = \rho U_{\max} H/\eta$ (ρ and η being the density and viscosity of the polymer solution, respectively), the ratio of solvent to solution viscosities β, and the Weissenberg number $W = \lambda U_{\max}/H$, where λ is the polymer relaxation time; below, we also use the elasticity number $E = W/\mathrm{Re}$ in lieu of W. The Oldroyd-B model regards the polymer molecules as noninteracting Hookean dumbbells, resulting in a shear-rate-independent viscosity and first normal stress coefficient in viscometric flows, and has been successfully used to predict linear and nonlinear instabilities in rectilinear [14,34,45] and both curvilinear viscometric [20,21,23] and nonviscometric [46] flows. For plane Poiseuille flow, whose stability is examined here, the laminar state is given by $U(z) = (1-z^2)$, with a first normal stress difference $T_{xx} - T_{zz} = 8(1-\beta)W^2 z^2$. We analyze its temporal stability by imposing infinitesimal 2D perturbations (justified by Squire's theorem [47]) to any dynamical variable, $f'(x,z,t)$, of the form $f'(x,z,t) = \tilde{f}(z)\exp[ik(x-ct)]$, where $\tilde{f}(z)$ is the eigenfunction, k is the streamwise wave number, and $c = c_r + ic_i$ is the complex wave speed, with the flow being temporally unstable when $c_i > 0$. Linearization results in a generalized eigenvalue problem [16,45] that is solved using spectral collocation and shooting methods, both of which have been extensively benchmarked [15,16,48].

We first consider the creeping-flow limit ($\mathrm{Re} = 0$) where the relevant dimensionless groups are W and β. In the absence of the solvent [$\beta = 0$; the upper-convected Maxwell (UCM) limit], the inertialess plane Poiseuille eigenspectrum is known [31] to contain six discrete modes for $W, k \sim O(1)$, in addition to the continuous spectrum (CS). As W is increased for a fixed $k \sim O(1)$ [or k is increased at a fixed $W \sim O(1)$], two of the modes merge into the CS, while two transition into "wall modes." The remaining two transition into "center modes" with phase speeds approaching the base-flow maximum. Regardless of W and k, however, plane Poiseuille flow of a UCM fluid remains stable [31]. For $\beta \neq 0$, the number of discrete modes depends on β, k, and W. For ultradilute solutions with $\beta > 0.99$, there are two center modes out of a total of five discrete modes for $W \sim O(10^3)$ and higher (see Fig. 1). Interestingly, for $\beta > 0.9905$, at sufficiently high $W \sim 2500$, one of the two center modes becomes unstable

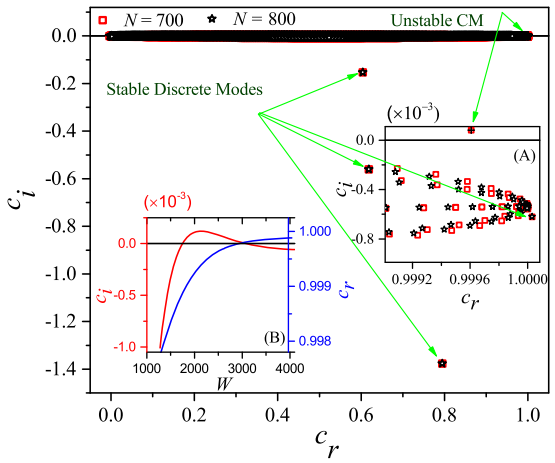

FIG. 1. The inertialess plane Poiseuille spectrum of an Oldroyd-B fluid shows five discrete modes for $\beta = 0.997$, $k = 0.75$, $W = 2500$, with three in the main figure and the remaining two visible in inset A; N is the number of Chebyshev polynomials in the spectral expansion. Inset A shows an enlarged view of the region near the unstable center mode ("unstable CM"). Inset B shows the variation of c_r and c_i with W. The detailed W dependence of the spectra is given in the Supplemental Material [49].

(inset A of Fig. 1; also see the Supplemental Material [49]). The instability runs counter to the prevailing view [31], and the unexpected destabilizing role of the solvent viscosity is similar to the recently discovered elasto-inertial center-mode instability [14–16].

The regime $W \sim O(10^3), \beta > 0.99$ corresponds to highly elastic ultradilute polymer solutions (with concentrations around 1% of the overlap value), one that was not explored in earlier theoretical work [31], but has been shown to be experimentally accessible in microscale flows [50–53]. Nevertheless, a concern arising from the large W's involved is the applicability of a simplified dumbbell approximation for the actual polymer molecules; earlier efforts [54–56] point to the need for more detailed microscopic models to faithfully capture the dynamics in the strongly nonlinear regime [57]. In this regard, it is worth noting that the recent effort of Buza *et al.* [58] has used the finitely extensible nonlinear elastic model with Peterlin closure (FENE-P) model to show that the Oldoyrd-B-based instability predicted here persists down to $W \sim O(100)$, allowing for a more concrete connection with experiments.

Neutral curves demarcate unstable "tongues" in the W-k plane (Fig. 2), with the tongues ceasing to exist beyond a critical k and below a threshold W. However, the instability continues to exist at arbitrarily small k, with $W \sim 1/k$ for $k \ll 1$ along both the branches of the tongue. A plot of W_c (the minimum W along a neutral curve) with $(1-\beta)$ (inset B of Fig. 2) shows that the lowest W_c is ~973.8 for $\beta = 0.994$, and that $W_c \propto (1-\beta)^{-1}$, $k_c \sim O(1)$ for $\beta \to 1$; expectedly, $W(1-\beta)k$ is the threshold parameter for $k, (1-\beta) \ll 1$; see inset A of Fig. 2 and [59]. The instability ceases to exist below $\beta = 0.9905$.

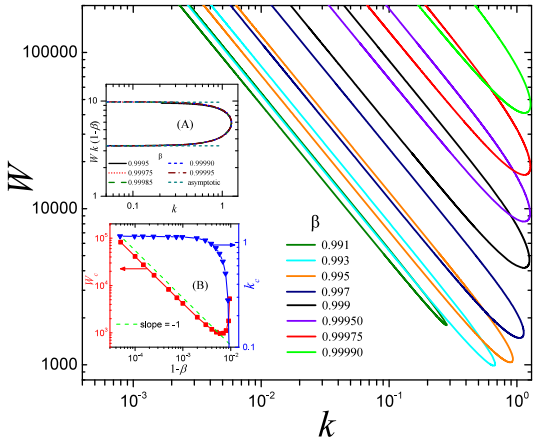

FIG. 2. Neutral curves in the W-k plane for different β's in the creeping-flow limit; inset A shows the collapse for $\beta \to 1$ when plotted as $Wk(1-\beta)$ vs k and the results obtained from the reduced equations in that limit. Inset B shows the variation of the critical Weissenberg number W_c and wave number k_c with $(1-\beta)$. Enlarged versions of the two insets are provided in the Supplemental Material [49].

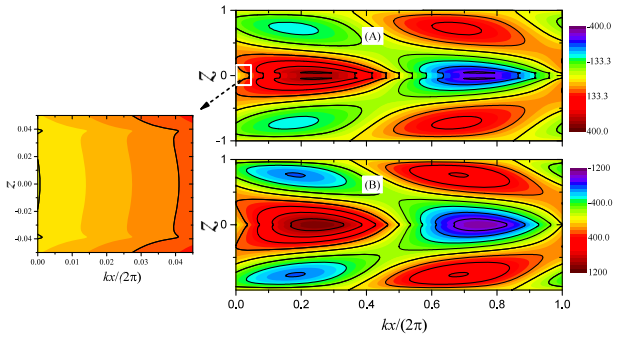

(a) Contours of v_x for $W(1-\beta) = 43$ (A) and 80 (B)

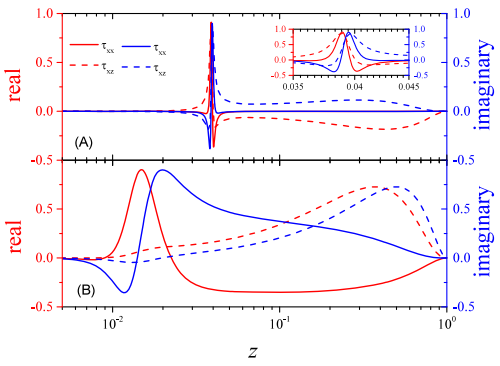

(b) $\tilde{\tau}_{xx}$ and $\tilde{\tau}_{xz}$ for $W(1-\beta) = 43$ (A) and 80 (B)

FIG. 3. The center-mode eigenfunctions for $W(1-\beta) = 43$, 80, $k = 0.08$ and $\mathrm{Re} = 0$, corresponding to neighborhood of the lower threshold and the center of the unstable region in the collapsed neutral curves shown in inset A of Fig. 2. The constant-amplitude contours of the streamwise velocity are shown in subfigure (a), while the eigenfunctions for τ_{xz} and τ_{xx} are shown in (b). The expanded region near the centerline for panel (A) in (a) is also shown.

Figure 3(a) shows contour plots for the streamwise velocity field alongside the polymeric stress eigenfunctions in Fig. 3(b) for $W(1-\beta)$'s near the lower threshold and close to the maximum growth rate (inset A of Fig. 2). The instability arises due to stretched polymers being rotated away from flow alignment by the perturbation shear, as they are swept past by the base-state parabolic flow. The differential rate of convection becomes small close to the centerline, owing to the phase speed of the eigenmode closely approaching the base-state maximum. As a result, the time available for the perturbation-shear-induced rotation (of the stretched polymers) increases, and the resulting accumulation of perturbation elastic shear stress (τ_{xz}) drives a reinforcing flow, leading to exponential growth. Close to neutrality, the stress (τ_{xx} and τ_{xz}) eigenfunctions, in particular [panel A of Fig. 3(b)], are seen to develop singular features in an $O(1/W)$ elastic critical layer, where the phase speed equals the local laminar velocity. The complicated eigenfunction structure near the lower threshold, as evident from the cusps close to the centerline [see magnified view in Fig. 3(a)], arises from competing influences of τ_{xz} (destabilizing, as mentioned above) and τ_{xx} (stabilizing).

The results above highlight a hitherto unknown center-mode instability in inertialess channel flow of an Oldroyd-B fluid for $\beta > 0.9905$, whereas in earlier efforts [14–16] we have identified a center-mode instability for $\mathrm{Re} \sim O(100)$ and $\beta \sim 0.9$, both for channel and pipe flows, and that may underlie the EIT state in these geometries [4,5,60]. The question arises, naturally, as to whether there is a connection between the elastic center mode identified here and the elasto-inertial one identified in Refs. [14–16]. Figure 4 shows the critical Reynolds number Re_c as a function of $E(1-\beta)$ and confirms such a connection. For $\beta \leq 0.9905$, the elasto-inertial instability [14] exhibits the scaling $\mathrm{Re}_c \propto [E(1-\beta)]^{-3/2}$ for $E(1-\beta) \ll 1$, reflecting the simultaneous importance of inertia, elasticity, and viscous effects in a thin layer near the channel centerline [14], with Re_c increasing sharply beyond a threshold $E(1-\beta)$. In stark contrast, for $\beta > 0.9905$, while Re_c initially decreases as $[E(1-\beta)]^{-3/2}$, there is an eventual crossover to $\mathrm{Re}_c \propto [E(1-\beta)]^{-1}$, with this scaling persisting down to arbitrarily small Re. The $\mathrm{Re}_c \propto E^{-1}$ scaling translates to an independence with respect to inertia and corresponds to the creeping-flow instability identified above, with $W(1-\beta)$ being the threshold parameter. While a connection between EIT and ET states has been conjectured [4,12,19], and the possibility of a common instability underlying these states speculated upon [39], ours is the first explicit demonstration of the same.

Interestingly, an intermediate scaling regime with $\mathrm{Re}_c \propto [E(1-\beta)]^{-1/2}$ emerges for a small window of β's

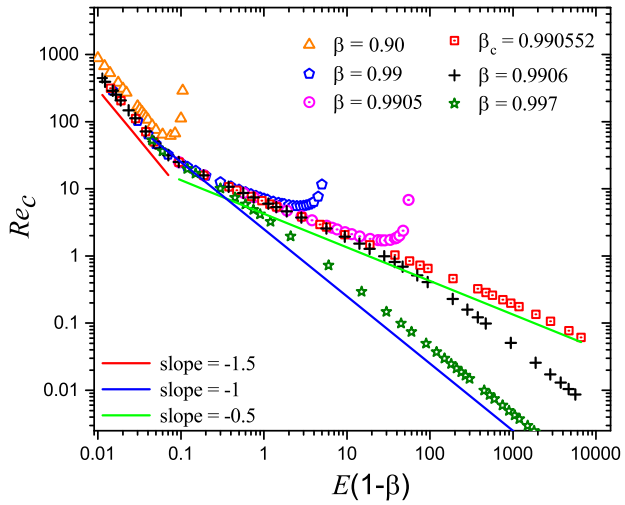

FIG. 4. The variation of critical Reynolds number Re_c with $E(1-\beta)$ for $\beta \geq 0.9$. For $\beta \leq 0.9905$, $\mathrm{Re}_c \propto [E(1-\beta)]^{-3/2}$ for small $E(1-\beta)$, but increases sharply beyond a critical $E(1-\beta)$. For $\beta > 0.9905$, while Re_c initially decreases as $[E(1-\beta)]^{-3/2}$, beyond a critical $E(1-\beta)$, there is a crossover to the scaling $\mathrm{Re}_c \propto [E(1-\beta)]^{-1}$. For $0.997 > \beta \geq 0.99$, there is an intermediate scaling regime with $\mathrm{Re}_c \propto [E(1-\beta)]^{-1/2}$; this regime persists down to $\mathrm{Re} \to 0$ for $\beta_c = 0.990552$.

around 0.9905. In this regime, the flow velocity $U \propto \{1/[(1-\beta)]\}U^0_{\mathrm{shear}}$, $U^0_{\mathrm{shear}} = \sqrt{\{[\eta(1-\beta)]/\lambda\rho\}}$ being the shear-wave speed in a quiescent fluid, pointing to an ostensible connection with observations of waves in recent experiments involving highly elastic polymer solutions at large W [51,52,61]. However, elastic shear waves in the strongly sheared laminar base state propagate with a speed of $O(E^{1/2}U)$ [62,63], precluding any such connection. The intermediate regime is absent for $\beta \geq 0.997$, so there is a direct transition from $\mathrm{Re}_c \propto [E(1-\beta)]^{-3/2}$ to $\mathrm{Re}_c \propto [E(1-\beta)]^{-1}$. Finally, continuity considerations imply that the β's where Re_c increases sharply, and those where Re_c transitions to an $[E(1-\beta)]^{-1}$ scaling for E's beyond the intermediate regime, are separated by a critical $\beta = \beta_c$ ($\approx$0.990552; see Fig 4) where, remarkably, the aforesaid intermediate scaling persists for $\mathrm{Re} \to 0$, $E \to \infty$.

Traditional research in Newtonian turbulence has been rooted in a statistical description aiming to explain, for instance, the subtle nature of small-scale universality at high Re, in a homogeneous isotropic setting [64–66]. The approach at moderate Re, especially from the perspective of understanding transition, has, however, undergone a paradigm shift with the advent of a dynamical systems perspective [67,68]. For wall-bounded rectilinear shearing flows, this latter approach is based on the dynamics of exact coherent structures that account for both an ambient shear and the presence of boundaries [68–72]. In contrast, theoretical efforts aimed at understanding the effect of elasticity on, for instance, the energy cascade in Newtonian turbulence, mirror the statistical approach above [73,74]. For elastic turbulence, such efforts have predicted a rapid decay, at least as fast as k^{-3} (k being the wave number), of the kinetic energy spectrum pointing to the spatially smooth character of small-scale elastic turbulent fluctuations, an aspect that has found experimental confirmation in curvilinear [17,18] and, to a lesser extent, in rectilinear flows [75]; see, however, [76]. There remains a dearth of information on the structural front primarily on account of earlier experiments being restricted to channels with a cross-sectional aspect ratio of unity [37–39]; recent experiments have explored the coherent structures underlying the ET state in channels with high-aspect-ratio cross sections [19,27,52,53].

Our discovery of a linear instability that spans the ET and EIT regimes (Fig. 4) helps significantly expand the above picture, opening up multiple avenues for future research. A linear elastic instability, with a physical origin genuinely different from the hoop-stress-based pathway in curvilinear shearing flows, offers a template for novel nonlinear elastic coherent structures that could shed light on the large-scale dynamics of the ET state; this would complement the aforementioned statistical approach tailored to the smallest scales. Such an approach also offers an alternative to prevailing efforts that analyze the elastic transition in rectilinear shearing flows, based on a bifurcation-from-infinity perspective [33–35], by expanding about a linearly stable eigenmode. The physical basis of the nonlinear expansion is intimately tied to the hoop-stress-based mechanism that leads to a linear instability in the curvilinear geometries. It is worth noting that these nonlinear analyses were restricted to the $\beta \to 0$ limit. As evident from Fig. 1 and the description of the eigenspectrum above (the stability of the UCM limit, in particular), the elastic eigenspectrum is sensitively dependent on β [49], and the validity of a $\beta \to 0$ analysis, for the experimentally relevant case of dilute solutions with $\beta \to 1$, is not obvious. An expansion about, or a numerical continuation from, the unstable eigenmode reported here, therefore, offers access to a much larger region in the viscoelastic parameter space comprising W, Re, and β. The connection, at higher Re, between a nonlinear EIT structure [12,13] and the underlying linear eigenfunction [14], also points to the likely success of a numerical continuation approach. Thus, nonlinear coherent structures will likely exist over a wider range of polymer concentrations and Weissenberg numbers than the restricted range [$\beta > 0.9905$, $W \sim O(1000)$] corresponding to the actual linear instability. This expectation is reinforced by the recent prediction [58] that the elastic instability identified in this Letter is likely subcritical.

*vshankar@iitk.ac.in
†sganesh@jncasr.ac.in

[1] R. R. Kerswell, Nonlinearity **18**, R17 (2005).

[2] B. Eckhardt, T. M. Schneider, B. Hof, and J. Westerweel, Annu. Rev. Fluid Mech. **39**, 447 (2007).
[3] K. Avila, D. Moxey, A. D. Lozar, D. Barkley, and B. Hof, Science **333**, 192 (2011).
[4] D. Samanta, Y. Dubief, M. Holzner, C. Schäfer, A. N. Morozov, C. Wagner, and B. Hof, Proc. Natl. Acad. Sci. U.S.A. **110**, 10557 (2013).
[5] G. H. Choueiri, J. M. Lopez, and B. Hof, Phys. Rev. Lett. **120**, 124501 (2018).
[6] B. Chandra, V. Shankar, and D. Das, J. Fluid Mech. **844**, 1052 (2018).
[7] G. H. Choueiri, J. M. Lopez, A. Varshney, S. Sankar, and B. Hof, arXiv:2103.00023.
[8] J. M. Lopez, G. H. Choueiri, and B. Hof, J. Fluid Mech. **874**, 699 (2019).
[9] A. Shekar, R. M. McMullen, S. N. Wang, B. J. McKeon, and M. D. Graham, Phys. Rev. Lett. **122**, 124503 (2019).
[10] A. Shekar, R. M. McMullen, B. J. McKeon, and M. D. Graham, J. Fluid Mech. **897**, A3 (2020).
[11] S. Sid, V. E. Terrapon, and Y. Dubief, Phys. Rev. Fluids **3**, 011301(R) (2018).
[12] J. Page, Y. Dubief, and R. R. Kerswell, Phys. Rev. Lett. **125**, 154501 (2020).
[13] Y. Dubief, J. Page, R. R. Kerswell, V. E. Terrapon, and V. Steinberg, arXiv:2006.06770.
[14] P. Garg, I. Chaudhary, M. Khalid, V. Shankar, and G. Subramanian, Phys. Rev. Lett. **121**, 024502 (2018).
[15] I. Chaudhary, P. Garg, G. Subramanian, and V. Shankar, J. Fluid Mech. **908**, A11 (2021).
[16] M. Khalid, I. Chaudhary, P. Garg, V. Shankar, and G. Subramanian, J. Fluid Mech. **915**, A43 (2021).
[17] A. Groisman and V. Steinberg, Nature (London) **405**, 53 (2000).
[18] A. Groisman and V. Steinberg, Nature (London) **410**, 905 (2001).
[19] V. Steinberg, Annu. Rev. Fluid Mech. **53**, 27 (2021).
[20] R. G. Larson, E. S. G. Shaqfeh, and S. J. Muller, J. Fluid Mech. **218**, 573 (1990).
[21] G. H. McKinley, J. A. Byars, R. A. Brown, and R. C. Armstrong, J. Non-Newtonian Fluid Mech. **40**, 201 (1991).
[22] A. Oztekin and R. A. Brown, J. Fluid Mech. **255**, 473 (1993).
[23] Y. L. Joo and E. S. G. Shaqfeh, J. Fluid Mech. **262**, 27 (1994).
[24] P. Pakdel and G. H. McKinley, Phys. Rev. Lett. **77**, 2459 (1996).
[25] E. S. G. Shaqfeh, Annu. Rev. Fluid Mech. **28**, 129 (1996).
[26] B. A. Schiamberg, L. T. Shereda, H. hu, and R. G. Larson, J. Fluid Mech. **554**, 191 (2006).
[27] Y. Jun and V. Steinberg, Phys. Rev. E **84**, 056325 (2011).
[28] A. Fouxon and V. Lebedev, Phys. Fluids **15**, 2060 (2003).
[29] T. C. Ho and M. M. Denn, J. Non-Newtonian Fluid Mech. **3**, 179 (1977).
[30] R. G. Larson, Rheol. Acta **31**, 213 (1992).
[31] H. J. Wilson, M. Renardy, and Y. Renardy, J. Non-Newtonian Fluid Mech. **80**, 251 (1999).
[32] V. Bertola, B. Meulenbroek, C. Wagner, C. Storm, A. Morozov, W. van Saarloos, and D. Bonn, Phys. Rev. Lett. **90**, 114502 (2003).
[33] B. Meulenbroek, C. Storm, A. N. Morozov, and W. van Saarloos, J. Non-Newtonian Fluid Mech. **116**, 235 (2004).
[34] A. N. Morozov and W. van Saarloos, Phys. Rev. Lett. **95**, 024501 (2005).
[35] A. N. Morozov and W. van Saarloos, Phys. Rep. **447**, 112 (2007).
[36] A. N. Morozov and W. van Saarloos, J. Stat. Phys. **175**, 554 (2019).
[37] L. Pan, A. Morozov, C. Wagner, and P. E. Arratia, Phys. Rev. Lett. **110**, 174502 (2013).
[38] B. Qin and P. E. Arratia, Phys. Rev. Fluids **2**, 083302 (2017).
[39] B. Qin, P. F. Salipante, S. D. Hudson, and P. E. Arratia, Phys. Rev. Lett. **123**, 194501 (2019).
[40] M. R. Jovanovic and S. Kumar, Phys. Fluids **22**, 023101 (2010).
[41] M. R. Jovanovic and S. Kumar, J. Non-Newtonian Fluid Mech. **166**, 755 (2011).
[42] M. Zhang, I. Lashgari, T. A. Zaki, and L. Brandt, J. Fluid Mech. **737**, 249 (2013).
[43] R. B. Bird, R. C. Armstrong, and O. Hassager, *Dynamics of Polymeric liquids, Vol. 1 Fluid Mechanics* (John Wiley, New York, 1977).
[44] R. G. Larson, *Constitutive Equations for Polymer Melts and Solutions* (Butterworths, London, 1988).
[45] R. Sureshkumar and A. N. Beris, J. Non-Newtonian Fluid Mech. **56**, 151 (1995).
[46] R. J. Poole, M. A. Alves, and P. J. Oliveira, Phys. Rev. Lett. **99**, 164503 (2007).
[47] A. Bistagnino, G. Boffetta, A. Celani, A. Mazzino, A. Puliafito, and M. Vergassola, J. Fluid Mech. **590**, 61 (2007).
[48] I. Chaudhary, P. Garg, V. Shankar, and G. Subramanian, J. Fluid Mech. **881**, 119 (2019).
[49] See Supplemental Material at http://link.aps.org/supplemental/10.1103/PhysRevLett.127.134502 for a detailed picture on the nature of the spectrum for $\beta \to 1$ as W is increased from $O(1)$ to $O(1000)$.
[50] K. P. Nolan, A. Agarwal, L. Shenghui, and R. Shields, Microfluid Nanofluid **20**, 101 (2016).
[51] A. Varshney and V. Steinberg, Phys. Rev. Fluids **3**, 103303 (2018).
[52] N. K. Jha and V. Steinberg, arXiv:2009.12258.
[53] R. Shnapp and V. Steinberg, arXiv:2106.01817.
[54] P. S. Doyle, E. S. G. Shaqfeh, and A. P. Gast, J. Fluid Mech. **334**, 251 (1997).
[55] P. S. Doyle and E. S. Shaqfeh, J. Non-Newtonian Fluid Mech. **76**, 43 (1998).
[56] R. Radhakrishnan and P. T. Underhill, Soft Matter **8**, 6991 (2012).
[57] Adopting a microscopic bead-rod model, Shaqfeh and coworkers [54,55] have illustrated the quantitative shortcomings of the FENE class of models. These shortcomings arise especially during transient dynamics of extensional flows when the imposed timescale becomes comparable to that characterizing equilibration in the underlying molecular configuration space.
[58] G. Buza, J. Page, and R. R. Kerswell, arXiv:2107.06191.
[59] The lower and upper threshold values of $Wk(1-\beta)$ for the instability are captured very well by a numerical solution of the reduced set of governing equations in this limit.

[60] S. S. Srinivas and V. Kumaran, J. Fluid Mech. **812**, 1076 (2017).
[61] A. Varshney and V. Steinberg, Nat. Commun. **10**, 652 (2019).
[62] J. M. Rallison and E. J. Hinch, J. Fluid Mech. **288**, 311 (1995).
[63] A. Roy, P. Garg, J. S. Reddy, and G. Subramanian, arXiv: 2101.00805.
[64] U. Frisch, *Turbulence: The Legacy of A. N. Kolmogorov* (Cambridge University Press, Cambridge, England, 1995).
[65] K. R. Sreenivasan and R. A. Antonia, Annu. Rev. Fluid Mech. **29**, 435 (1997).
[66] K. R. Sreenivasan, Rev. Mod. Phys. **71**, S383 (1999).
[67] D. Barkley, J. Fluid Mech. **803**, P1 (2016).
[68] N. B. Budanur, K. Y. Short, M. Farazmand, A. P. Willis, and P. Cvitanović, J. Fluid Mech. **833**, 274 (2017).
[69] F. Waleffe, Phys. Rev. Lett. **81**, 4140 (1998).
[70] F. Waleffe, J. Fluid Mech. **435**, 93 (2001).
[71] H. Wedin and R. R. Kerswell, J. Fluid Mech. **508**, 333 (2004).
[72] A. P. Willis, K. Y. Short, and P. Cvitanović, Phys. Rev. E **93**, 022204 (2016).
[73] E. Balkovsky, A. Fouxon, and V. Lebedev, Phys. Rev. Lett. **84**, 4765 (2000).
[74] E. Balkovsky, A. Fouxon, and V. Lebedev, Phys. Rev. E **64**, 056301 (2001).
[75] D. Bonn, F. Ingremeau, Y. Amarouchene, and H. Kellay, Phys. Rev. E **84**, 045301(R) (2011).
[76] There is less consensus on the robustness of the $O(k^{-3})$ decay of the energy spectrum, and thence, the universality of the small scales of the elastic turbulence, since experiments have found some variation of the exponent between rectilinear [38] and curvilinear geometries, and even across different curvilinear geometries [17,18].